https://dx.doi.org/10.1016/j.energy.2021.122546

Radiative cooling-assisted thermoelectric refrigeration and power systems: coupling properties and parametric optimization

Tianjun Liao[a, b], Qidong Xu [a], Yawen Dai [a], Chun Cheng [a], Qijiao He [a], Meng Ni[a*]

[a] *Department of Building and Real Estate, Research Institute for Sustainable Urban Development (RISUD) and Research Institute for Smart Energy (RISE), The Hong Kong Polytechnic University, Hung Hom, Kowloon, Hong Kong, China*

[b] *Department of Physics and Energy, Chongqing Key Laboratory of Green Energy Materials Technology and Systems,Chongqing University of Technology, Chongqing 400054, China*

Abstract: A CP2–127–06 Melcor module is incorporated into a radiative cooling (RC) system to work as a thermoelectric refrigerator (TER) at daytime and a thermoelectric generator (TEG) in nighttime. Through analysis of the single RC system, only a small temperature span between environment and building can be achieved. However, the temperature span can be significantly improved by combining RC and TER. The TER's input electrical current is optimized to obtain the maximum coefficient of performance (COP) 4.85 and the maximum cooling power density (CPD) 9.64×10^3 W·m^{-2}. Making trade-off between COP and CPD, the optimal regions of the COP, CPD, temperatures of cold side and hot side, and electrical current are determined. Further, the RC-TEG system's maximum power density 5.10 W·m^{-2} and maximum efficiency 0.369% and the corresponding optimal conditions are obtained. With increasing the area ratio of emitter to TER or TEG, the performances of the systems are firstly improved and then remain almost unchanged. This work may provide guidance for building's thermal management at daytime and power generation in nighttime.

Key words: Radiative cooling; Thermoelectric refrigerator (TER); Thermoelectric generator

*Corresponding author (M. Ni)
Email: meng.ni@polyu.edu.hk; Tel: 852-27664152; Fax: 852-27645131

(TEG); Thermal-electrical properties; Atmospheric window

Nomenclature

A	area (m^2)
c	velocity of light ($\mathrm{m}\cdot\mathrm{s}^{-1}$)
E_{BB}	intensity of blackbody ($\mathrm{W}\cdot\mathrm{m}^{-2}\cdot\mathrm{nm}^{-1}$)
$E_{\mathrm{AM1.5}}$	solar irradiation intensity ($\mathrm{W}\cdot\mathrm{m}^{-2}\cdot\mathrm{nm}^{-1}$)
h	Planck constant ($\mathrm{eV}\cdot\mathrm{s}$)
I	electrical current (A)
k_{B}	Boltzmann constant ($\mathrm{J}\cdot\mathrm{K}^{-1}$)
K	thermal conductance ($\mathrm{W}\cdot\mathrm{K}^{-1}$)
l	length (m)
n	number of p-n couple
P	power (W)
p	power output density ($\mathrm{W}\cdot\mathrm{m}^{-2}$)
$\dot{Q}$	heat flow (W)
q	heat flow per unit area ($\mathrm{W}\cdot\mathrm{m}^{-2}$)
R	internal resistance of TER/TEG (Ω)
R_{L}	load resistance of TEG (Ω)
T	temperature (K)
t	transmittance
U	heat transfer coefficient ($\mathrm{W}\cdot\mathrm{m}^{-2}\cdot\mathrm{K}^{-1}$)
V	voltage (V)

Greek symbols

α	Seebeck coefficient ($\mathrm{V}\cdot\mathrm{K}^{-1}$)
β	structure parameter (m)
ρ	electrical resistivity ($\Omega\cdot\mathrm{m}$)
κ	thermal conductivity ($\mathrm{W}\cdot\mathrm{K}^{-1}\cdot\mathrm{m}^{-1}$)
λ	wavelength of photon (m)
ψ	coefficient of performance
ε	emissivity
η	efficiency
θ	angle

Subscript

A	ambient temperature
avg	average
atm	atmospheric
B	Building temperature
BB	black-body
cf	cut-off
H	hot side
L	cold side
m	maximum
n	n type semiconductor
non-rad	non-radiative
Rad	radiative
p	p type semiconductor
S	selective emitter
T	thermoelectric
sun	sunlght
su	start-up

Abbreviations

COP	coefficient of performance
CPD	cooling power density
RC	radiative cooling
RSC	radiative sky cooler
TEG	thermoelectric generator
TER	thermoelectric refrigerator

1. Introduction

Radiative cooling (RC) is a novel technology that ejects the infrared radiation from the heat source to the outer space through the atmospheric window (8～13 μm) that coincides with the black-body radiation of objects around 300 K [1, 2]. The surface of the thermal emitter receives solar energy and atmospheric radiation, emit infrared radiation, and simultaneously exchange non-radiative heat with the environment through thermal conduction and convection [3]. The RC technology has potential application in dealing with energy consumption and environmental problems caused by traditional refrigeration equipments, resulting tremendous attention on it. Generally, in order to make the RC system efficiently cool the object, researchers try to increase the reflection of sunlight and the thermal emissivity in the atmospheric window through material selection and structural optimization design [4]. Recently, researchers combined RC technology with photovoltaic (PV) panel [5, 6], thermoelectric refrigerators (TERs) [7, 8], and thermoelectric generators (TEGs) [9-14] to propose new conceptual thermal management and power generation systems. The PV panel, TER, and TEG covered a layer of selective emitter can enhance the emissivity in the mid-to-far infrared band, thereby decreasing the temperature. Zhao *et. al.* [5] experimentally and numerically studied the RC–PV system that can produce electricity at daytime by PV panel and obtain cooling power density in nighttime by RC system simultaneously. The daily average power generation, electrical efficiency, and cooling power of the PV–RC system were measured. Kwan *et. al.* [8] integrated the radiative sky cooler (RSC) with TER to form the hybrid cooling system that can reduce the TER power consumption and increase the system's cooling capacity over a standalone RSC. A metric to

define the degree of TER power consumption reduction due to the RSC. The effects of the TER module type, the RSC surface area and radiative emissivity value, solar absorption coefficient and air convective heat transfer coefficient on the system's cooling capacity and the TER power saving coefficient. It has been demonstrated that increasing the RSC surface area further improved the TER power saving coefficient, but the solar absorption coefficient had to be under 0.02 to maintain a reasonable TER power saving coefficient. Ishii *et. al.* [9] integrated a wavelength selective emitter on the TEG to achieve continuous power generation at daytime and in nighttime. The results demonstrated that the top of the TEG is colder than the bottom, causing the generation of temperature difference and voltage under various weather conditions. The electricity can be applied in special equipments (e.g. semiconductor LED lighting) and off-grid areas. Liu *et. al.* [12] analyzed the adverse impact of ambient temperature and atmospheric humidity, and the positive impact of solar absorption and wind speed on the RC-TEG system. The developed RC-TEG system achieved a maximum power density of 0.92 $W \cdot m^{-2}$ and significantly improved the all-day power generation performance. Mu *et. al.* [13] fabricated a multilayer thermal emitter on the surface of a TEG to achieve heat-to-electricity conversion by means of the RC. The experiment demonstrated that the maximum temperature span between the hot- and cold-sides of the TEG can reach up to 4 K, the output voltage of the RC-TEG can reach up to 0.5 mV, and the RC-TEG presented a continuous average 0.18 mV output for 24 h. Compared to a pure Al heat sink, Zhan *et. al.* [14] improve the TEG's electricity about 55%–70% for temperature range of 150～250 by using the passive RC associated with nano-porous alumina on aluminum surfaces. Jalil *et. al.* [15, 16] enhanced the temperature difference across the TEG module over a wide temperature

range by using high-intensity and ultrafast pulsed fs-laser as a heat sink on the cold side of the TEG and the combined effect of the enhanced radiative and convective cooling.

Although researchers enhanced the performances of TEG and the TER with the help of RC materials, the temperature dependence of the physical properties of TE materials are not considered, and the electrical parameters, thermal parameters, and structural parameters are not optimized to obtain the optimum performance. In this work, the thermal-optical-electrical coupling characteristics of the system are further investigated to provide theoretical basis for the production of practical systems.

2. Model description of a RC-TER system

The schematic diagram of a RC-TER system is illustrated in Fig. 1(a), where the wavelength selective emitter and the TER are, respectively, placed on top and bottom of the system. The Bi_2Te_3 material based CP2–127–06 Melcor module works as a TER [17]. A 1-mm-thick lithium fluoride crystal coated with silver backing forms the selective emitter that presents a low solar absorptance and nearly ideal infrared selectivity with high emission exactly within the atmospheric window [18]. The work principle is described as follows. At the daytime, the sunlight is selectively absorbed on the emitter's surface, which simultaneously exchanges radiative heat with the outer space through the atmospheric window to achieve the thermal management. P_{rad}, P_{sun}, P_{atm}, and $P_{\text{non-rad}}$ are the radiated power from the emitter at the temperature T_{S}, the absorbed power from the incident sunlight, the absorbed power from the atmospheric radiation at the temperature T_{atm}, and the convective heat exchange between the emitter and the environment. The TER operates at two different temperatures T_{H} and T_{L} as external voltage V is imposed on it. The electrical

current I enters into the TER leads that the hot side and cold side release and absorb heat flows $\dot{Q}_{\mathrm{H}}$ and $\dot{Q}_{\mathrm{L}}$, respectively. The Building's temperature can be significantly decreased with help of the TER. The spectral dependent emissivities of the selective emitter and the AM1.5G solar spectrum are shown in Fig. 1(c) [18]. As the wavelength locates in the range of $280 \sim 4000$ nm, the absorptivities (emissivities) are small, while the emissivities in the atmospheric transmission window too relatively large. Designers are committed to designing suitable materials or structures to increase the reflection of sunlight and the radiative emission in the atmospheric transmission window.

2.1. The thermal properties of the RC system

According to the energy balance analysis, the net power entering the selective absorber is determined by [1, 2]

$$P_{\mathrm{net}} = P_{\mathrm{sun}} + P_{\mathrm{atm}}\left(T_{\mathrm{atm}}\right) + P_{\mathrm{non\text{-}rad}} - P_{\mathrm{rad}}\left(T_{\mathrm{S}}\right). \tag{1}$$

The power P_{sun} absorbed from the sunlight is expressed as [1, 2]

$$P_{\mathrm{sun}} = \int_0^{\infty} d\lambda E_{\mathrm{AM1.5}}\left(\lambda\right)\varepsilon\left(\lambda\right)\cos\theta, \tag{2}$$

where $E_{\mathrm{AM1.5}}\left(\lambda\right)$ is the solar spectral irradiation intensity of AM 1.5G. $\varepsilon\left(\lambda\right)$ denotes the emissivity of the selective emitter.

The radiative power density $P_{\mathrm{rad}}\left(T_{\mathrm{S}}\right)$ emitted from the selective emitter is [1, 2]

$$P_{\mathrm{rad}}\left(T_{\mathrm{S}}\right) = \int d\Omega\cos\theta\int_0^{\infty} d\lambda E_{\mathrm{BB}}\left(T_{\mathrm{S}},\lambda\right)\varepsilon_{\mathrm{rad}}\left(\lambda,\theta\right), \tag{3}$$

where $\varepsilon_{\mathrm{rad}}\left(\lambda,\theta\right)$ is the spectral angular emissivity. Ω is an integral over the hemispherical solid angle, i.e., [1, 2]

$$\int d\Omega = \int_0^{\pi/2} d\theta\sin\theta\int_0^{2\pi} d\varphi, \tag{4}$$

where $E_{\mathrm{BB}}\left(T,\lambda\right)$ is the intensity of a blackbody at temperature T, i.e.,

$$E_{\mathrm{BB}}(T,\lambda)=\left(\frac{2hc^2}{\lambda^5}\right)\left\{\exp\left[\frac{hc}{\lambda k_{\mathrm{B}}T}\right]-1\right\}^{-1}, \tag{5}$$

where k_{B} is the Boltzmann constant. λ denotes the wavelength of the photon. h stands for the Planck's constant. c accounts for the light's velocity.

By replacing the absorptivity of the selective emitter with its emissivity $\varepsilon(\lambda,\theta)$ based on Kirchhoff's law, the absorbed power density $P_{\mathrm{atm}}(T_{\mathrm{atm}})$ from the atmosphere is given by [1]

$$P_{\mathrm{atm}}(T_{\mathrm{atm}})=\int d\Omega\cos\theta\int_0^{\infty}d\lambda E_{\mathrm{BB}}(T_{\mathrm{atm}},\lambda)\varepsilon(\lambda,\theta)\varepsilon_{\mathrm{atm}}(\lambda,\theta), \tag{6}$$

where $\varepsilon_{\mathrm{atm}}(\lambda,\theta)$ is the spectral angular emittance of the atmosphere, which is closely related to factors such as atmospheric water content, aerosol conditions, and cloud cover.

Based on Kirchhoff law and the Beer–Lambert law, the angular emissivity $\varepsilon_{\mathrm{atm}}(\lambda,\theta)$ of the atmosphere is determined as [19]

$$\varepsilon_{\mathrm{atm}}(\lambda,\theta)=1-t_{\mathrm{atm}}(\lambda,0)^{1/\cos\theta}, \tag{7}$$

where $t_{\mathrm{atm}}(\lambda,0)$ is the atmospheric transmittance in the zenith direction [19].

Based on the Newton's heat transfer law, the thermal power entering the emitter is assumed to have the form

$$P_{\text{non-rad}}(T_{\mathrm{A}},T_{\mathrm{S}})=U(T_{\mathrm{A}}-T_{\mathrm{S}}), \tag{8}$$

where $T_{\mathrm{A}}=300\,\mathrm{K}$ is the ambient temperature. The natural convective heat transfer coefficient U locates in the range of $2\sim10\ \mathrm{W\cdot m^{-2}\cdot K^{-1}}$.

2.2. The electrical-thermal properties of the TER

Electrical current flowing through the TER generates Joule heat and leads that one side absorbs heat and the other side releases heat due to the Peltier effect, which causes a temperature difference between cold and hot sides. Meanwhile, Fourier heat transfer is occurred. Considering the Peltier, Fourier, and Joule effects, the heat flow $\dot{Q}_{\mathrm{L}}$ from the

cooling space to the TER and the heat flow $\dot{Q}_{\mathrm{H}}$ from the TER to the environment can be calculated as [20-22]

$$\dot{Q}_{\mathrm{L}} = \alpha T_{\mathrm{L}} I - K\left(T_{\mathrm{H}} - T_{\mathrm{L}}\right) - \frac{1}{2} I^2 R \tag{9}$$

and

$$\dot{Q}_{\mathrm{H}} = \alpha T_{\mathrm{H}} I - K\left(T_{\mathrm{H}} - T_{\mathrm{L}}\right) + \frac{1}{2} I^2 R, \tag{10}$$

where $\alpha = n\left(\alpha_{\mathrm{p}} - \alpha_{\mathrm{n}}\right)$, $K = n\beta\left(\kappa_{\mathrm{p}} + \kappa_{\mathrm{n}}\right)$, and $R = n\beta^{-1}\left(\rho_{\mathrm{p}} + \rho_{\mathrm{n}}\right)$ are, respectively, the TER's Seebeck coefficient, thermal conductance, and internal resistance. The subscripts n and p represent n- and p-type elements. n is the number of p-n couple. For convenience of discuss, a structure parameter $\beta = A_{\mathrm{p}}/l_{\mathrm{p}} = A_{\mathrm{n}}/l_{\mathrm{n}}$ is introduced. A and l are, respectively, the cross-sectional area and the length of an semiconductor element. ρ and κ are, respectively, the resistivity and the thermal conductivity. The dependences of a p-n couple's Seebeck coefficient, resistivity, and thermal conductivity on the mean temperature T_{avg} are constrained by using equations as [20-22]

$$\alpha_{\mathrm{p}} - \alpha_{\mathrm{n}} = \left(22224 + 930.6T_{\mathrm{avg}} - 0.9905T_{\mathrm{avg}}^2\right) \times 10^{-9}, \tag{11}$$

$$\rho_{\mathrm{p}} + \rho_{\mathrm{n}} = \left(5112 + 163.4T_{\mathrm{avg}} + 0.6279T_{\mathrm{avg}}^2\right) \times 10^{-10}, \tag{12}$$

and

$$\kappa_{\mathrm{p}} + \kappa_{\mathrm{n}} = \left(62605 - 277.7T_{\mathrm{avg}} + 0.4131T_{\mathrm{avg}}^2\right) \times 10^{-4}, \tag{13}$$

where $T_{\mathrm{avg}} = 0.5\left(T_{\mathrm{H}} + T_{\mathrm{L}}\right)$.

The boundaries of TER obey Newton's law of heat transfer, and thus, two equations are given by [21]

$$\dot{Q}_{\mathrm{L}} = U_{\mathrm{L}} A_{\mathrm{L}} \left(T_{\mathrm{B}} - T_{\mathrm{L}}\right) \tag{14}$$

and

$$\dot{Q}_{\mathrm{H}} = U_{\mathrm{H}} A_{\mathrm{H}} \left(T_{\mathrm{H}} - T_{\mathrm{S}} \right). \tag{15}$$

where A_{L} and A_{H} are the heat exchange areas. The heat transfer coefficients $U_{\mathrm{L}} A_{\mathrm{L}} = 7.48\,\mathrm{W \cdot K^{-1}}$ and $U_{\mathrm{H}} A_{\mathrm{H}} = 8.09\,\mathrm{W \cdot K^{-1}}$ are chosen [19]. The CP2–127–06 Melcor module's front surface area A_{T} is equal to $3.6 \times 10^{-3}\,\mathrm{m^2}$. We set $A_{\mathrm{L}} = A_{\mathrm{H}} = A_{\mathrm{T}}$ in this work.

According to Eqs. (9) and (10), the input power P_{T} of the TER can be obtained as

$$P_{\mathrm{T}} = \dot{Q}_{\mathrm{H}} - \dot{Q}_{\mathrm{L}} = \alpha \left(T_{\mathrm{H}} - T_{\mathrm{L}} \right) I + I^2 R = VI\,, \tag{16}$$

where $V = \alpha \left(T_{\mathrm{H}} - T_{\mathrm{L}} \right) + IR$ is the input voltage on the TER. It can be found from Eqs. (9)-(16) that the TER's physics properties closely depend on the temperatures T_{H} and T_{L}, which should be obtained by solving the energy balance equations.

2.3. The power output and efficiency of the RC-TEC and TEG systems

When the system is in operation at steady state, an energy balance equation is given by

$$A_{\mathrm{S}} \left[P_{\mathrm{sun}} + P_{\mathrm{atm}} \left(T_{\mathrm{atm}} \right) - P_{\mathrm{rad}} \left(T_{\mathrm{S}} \right) \right] + \left(2 A_{\mathrm{S}} - A_{\mathrm{T}} \right) P_{\mathrm{non\text{-}rad}} = P_{\mathrm{T}}\,, \tag{17}$$

where A_{S} is the front surface area of the selective emitter.

By using $A_{\mathrm{H}} = A_{\mathrm{T}}$, Eq. (17) can be rewritten as

$$\left(A_{\mathrm{S}} / A_{\mathrm{T}} \right) \left[P_{\mathrm{sun}} + P_{\mathrm{atm}} \left(T_{\mathrm{atm}} \right) - P_{\mathrm{rad}} \left(T_{\mathrm{S}} \right) \right] + \left(2 A_{\mathrm{S}} / A_{\mathrm{T}} - 1 \right) P_{\mathrm{non\text{-}rad}} = U_{\mathrm{H}} A_{\mathrm{T}} \left(T_{\mathrm{H}} - T_{\mathrm{S}} \right). \tag{18}$$

Using Eqs. (9) and (16), the coefficient of performance (COP) ψ can be expressed as

$$\psi = \frac{\dot{Q}_{\mathrm{L}}}{P_{\mathrm{T}}} = \frac{\alpha T_{\mathrm{L}} I - K \left(T_{\mathrm{H}} - T_{\mathrm{L}} \right) - 0.5 I^2 R}{\alpha \left(T_{\mathrm{H}} - T_{\mathrm{L}} \right) I + I^2 R}. \tag{19}$$

For a fixed electrical current I, one can obtain the temperatures T_{H} and T_{L} by solving Eqs. (9)-(15), and (18). Inserting I, T_{H}, and T_{L} into Eqs. (9) and (19), the cooling power density (CPD) Q_{L} and the COP ψ can be obtained.

3. Performance evaluation and parametric optimization

3.1 Model validation

Based on the experimental work from Ref. [18], the measured temperatures of the LiF-based RC cooler can be obtained. In the presence of the TER, the theoretical temperature temperatures of the LiF-based RC cooler can be calculated by using Eqs. (1)-(8). In Fig. 2(a), we can find that the theoretical temperature is very close to the measured temperature. Further, the TER's COP ψ and volt-ampere characteristics can be obtained according to the product information from Ref. [17]. The curves of the COP ψ and input voltage V as functions of electrical current I can be plotted by using Eqs. (9)-(16) and (19). We can find from Fig. 2(b) that the difference between the experimental curve and the theoretical curve is small. Therefore, the established RC-TER/TEG hybrid systems in this work are valid.

3.2 The single RC system

In the absence of the TER, only the single RC system can manage the temperature of the cooling space. For a fixed $U = 5\,\mathrm{W\cdot m^{-2}\cdot K^{-1}}$, the emitter's critical temperature $T_{\mathrm{C}} = 290.5\,\mathrm{K}$ is calculated numerically by setting $P_{\mathrm{net}} = 0\,\mathrm{W\cdot m^{-2}}$ in Eq. (1), which shows that the temperature difference between the emitter and the environment is 17.35 K. Although the purpose of the cooling is achieved, the small temperature span limits the application of the RC system. As the single RC system operates in nighttime, the emitter's critical temperature $T_{\mathrm{C}} = 286.0\,\mathrm{K}$ is calculated numerically by setting $P_{\mathrm{net}} = 0\,\mathrm{W\cdot m^{-2}}$ and $P_{\mathrm{sun}} = 0\,\mathrm{W\cdot m^{-2}}$ in Eq. (1). By varying the natural connective coefficient U, we can obtain different values of T_{C} through above similar method, as shown in Fig. 3. Making comparisons, we can find that the RC system's critical temperature span in nighttime is much larger than that at daytime. Fig. 3 shows that the critical temperature T_{C} increases with

increasing of U, the increase rates of critical temperature at daytime is much less than those in nighttime. Because the larger the air convective coefficient is, the more non-radiative heat flow enters into the system, resulting in the higher critical temperature is presented. What's more, the results reveal that the lower the non-radiative heat transfer, the better performance can exhibit. Because the emitter with high emissivity in the range of the atmospheric window and small emissivity outside the atmospheric window can improve performance, and thus, the emitter material selection and structure optimal design are of great importance for the RC system. Additionally, the weather conditions also influence the performance of the RC system. In the case of a clear sky, the lower the content of water vapor in the atmosphere is, the better performance can present. In the next section, we will study the thermal-electrical coupling properties of the RC-TER and the RC-TEG systems.

3.3 The RC-TER system

The dependences of T_{L} and T_{H} on the electrical current I are shown in Fig. 3(a). The numerical results reveal that the temperature of the TER's cold side is very close to that of the cooling space due to the selection of material with high heat coefficient. Therefore, the variation tendency of building's temperature with electrical current are similar with those of the TER's cold side. In order to make comparisons, the emitter's critical temperature T_{C} is plotted in Fig. 4(a). Fig. 4(a) depicts that the temperature T_{L} firstly decreases and then increases with the electrical current I, while the temperature T_{H} is a monotonically increasing function of the electrical current I. We can find from Fig. 4(a) that the temperatures T_{L} are larger than the critical temperature T_{C} as the electrical current I in the regions of $I < I_{\mathrm{su}}$ and $I > I_{\mathrm{cf}}$, where I_{su} and I_{cf} are, respectively, the star-up and

cut-off electrical currents. Apparently, the electrical current I should be operated in the region of $I_{\mathrm{su}} \le I \le I_{\mathrm{cf}}$. Fig. 4(b) shows that the curves of the COP ψ and the cooling power density (CPD) $q_{\mathrm{L}} = \dot{Q}_{\mathrm{L}} / A_{\mathrm{T}}$ as a function of I. Fig. 4(b) shows that the COP attains the maximum value $\psi_{\mathrm{m}} = 4.85$ at $I_{\psi} = 0.72$ A, while the CPD attains the maximum value $q_{\mathrm{L,m}} = 9.64 \times 10^{3}\ \mathrm{W \cdot m^{-2}}$ at $I_{q} = 7.61$ A. Combining Fig. 4(a) with Fig. 4(b), one can find that the temperature T_{L} attains the minimum value $T_{\mathrm{L,q}}$ at $q_{\mathrm{L,m}}$. By using the value of I_{ψ}, the temperatures $T_{\mathrm{L},\psi} = 289.6$ K and $T_{\mathrm{H},\psi} = 295.4$ K can be determined. By using the value of I_{q}, the temperatures $T_{\mathrm{L,q}} = 285.36$ K and $T_{\mathrm{H,q}} = 330.5$ K can be determined. Because the optimal value I_{ψ} is close to the star-up current I_{su}, the temperatures $T_{\mathrm{L},\psi}$ and $T_{\mathrm{H},\psi}$ are, respectively close to the critical temperature T_{C} and the building temperature T_{B}. Fig. 4(c) shows the curve of the CPD q_{L} as a function of COP ψ can be plotted. As depicted in Fig. 4(c), the CPD is equal to $q_{\mathrm{L},\psi}$ at the maximum COP point; the COP is equal to ψ_{q} at the maximum CPD point. Because small CPD at ψ_{m} and small COP at $q_{\mathrm{L,m}}$ are presented, thereby the CPD and the COP should be situated in the regions of

$$q_{\mathrm{L},\psi} \le q_{\mathrm{L}} \le q_{\mathrm{L,m}} \tag{20}$$

and

$$\psi_{\mathrm{q}} \le \psi \le \psi_{\mathrm{m}}. \tag{21}$$

The electrical current I and the temperatures T_{L} and T_{H} should locate in the regions of

$$I_{\psi} \le I \le I_{q}, \tag{22}$$

$$T_{\mathrm{L,q}} \le T_{\mathrm{L}} \le T_{\mathrm{L},\psi}, \tag{23}$$

and

$$T_{\mathrm{H},\psi} \le T_{\mathrm{H}} \le T_{\mathrm{H,q}}. \tag{24}$$

The effects of the area ratio A_S/A_T on the thermal-electrical properties of the RC-TER system are revealed in Fig. 4, where the shaded areas represent the optimal regions. Fig. 5 depicts that the small values of A_S/A_T have significant influences on ψ_m, I_ψ, $q_{L,m}$, I_q, etc., while the maximum COP and the CPD and the relevant parametric optimal values nearly keep at constants in the region of large area ratio. As we design the practical RC-TER system, the appropriate area ratio A_S/A_T can be selected due to the requirements of the cooling temperature span between the TER's cold side and the environment.

For nighttime operation, the maximum value $\psi_m = 15.7$ at $I_\psi = 0.24$ A and the maximum value $q_{L,m} = 1.02\times10^4\ \mathrm{W\cdot m^{-2}}$ at $I_q = 7.61$ A can be abstained by using above similar method. Because no power is absorbed from the incident sunlight at nighttime, one can find that the performances of the RC-TER system at nighttime are better that those of the RC-TER system at daytime.

3.4 The RC-TEG system

As the CP2–127–06 Melcor module works as a TEG, the output voltage can be generated. The TEG operates between two thermal reservoirs of the environment and outer space, absorbing heat $\dot{Q}_H$ from the environment and releasing heat $\dot{Q}_L$ to the outer space per unit time. Therefore, Eqs. (9) and (10) should be rewritten as [18, 19]

$$\dot{Q}_L = \alpha T_L I + K\left(T_H - T_L\right) + \frac{1}{2}I^2R \tag{25}$$

and

$$\dot{Q}_H = \alpha T_H I + K\left(T_H - T_L\right) - \frac{1}{2}I^2R, \tag{26}$$

Based on Eqs. (25) and (26), the heat-to-electricity conversion efficiency η and the power output density p of the TEG can be derived as

$$\eta = \frac{\dot{Q}_{\mathrm{H}} - \dot{Q}_{\mathrm{L}}}{\dot{Q}_{\mathrm{H}}} = \frac{\alpha\left(T_{\mathrm{H}} - T_{\mathrm{L}}\right)I - I^2 R}{\alpha T_{\mathrm{H}} I + K\left(T_{\mathrm{H}} - T_{\mathrm{L}}\right) - 0.5 I^2 R} \tag{27}$$

and

$$p = \frac{\dot{Q}_{\mathrm{H}} - \dot{Q}_{\mathrm{L}}}{A_{\mathrm{T}}} = \frac{\alpha\left(T_{\mathrm{H}} - T_{\mathrm{L}}\right)I - I^2 R}{A_{\mathrm{T}}}. \tag{28}$$

Eqs. (15) and (16) should be rewritten as

$$\dot{Q}_{\mathrm{L}} = U_{\mathrm{L}} A_{\mathrm{L}}\left(T_{\mathrm{L}} - T_{\mathrm{S}}\right) \tag{29}$$

and

$$\dot{Q}_{\mathrm{H}} = U_{\mathrm{H}} A_{\mathrm{H}}\left(T_{\mathrm{B}} - T_{\mathrm{H}}\right). \tag{30}$$

As the TEG operates in nighttime, an energy balance equation can be expressed as

$$A_{\mathrm{S}}\left[P_{\mathrm{rad}}\left(T_{\mathrm{S}}\right) - P_{\mathrm{atm}}\left(T_{\mathrm{atm}}\right)\right] - \left(2A_{\mathrm{S}} - A_{\mathrm{T}}\right)P_{\text{non-rad}} = \dot{Q}_{\mathrm{L}}. \tag{31}$$

By solving Eqs. (25), (26), (29), (30), and (31), the temperatures T_{H} and T_{L} can be determined for given values β and I. Inserting β, I, T_{H}, and T_{L} into Eqs. (25) and (26), the output voltage $V = \alpha\left(T_{\mathrm{H}} - T_{\mathrm{L}}\right) - IR$, the efficiency η and the power density p of the TEG can be obtained, as shown in Fig. 6. It is seen from Fig. 6(a) that the output voltage V firstly increases and then decreases with increase of β, which indicates that we can obtain a local maximum value of the output voltage. Further, Fig. 6(a) displays that the output voltage V is a monotonically increasing function of I, this volt-ampere characteristics determine that one can a pair of parameters (V, I) to maximize the power density and efficiency, as verified in Figs. 6(b) and 6(c). Consequently, we can obtain the maximum power density $p_{\max}$ and the maximum efficiency $\eta_{\max}$ and the parametric optimum values of β and I. Figs. 6(b) and 6(c) illustrate that the parametric optimum values of β and I at $p_{\max}$ are different from those at $\eta_{\max}$, which is caused by the irreversible thermal losses

inside and outside the TEG. For a given $A_S/A_T = 100$, the maximum power density $p_{max} = 5.10\,W\cdot m^{-2}$ and the optimal values $\beta_p = 3.84\times10^{-3}\,m$, $V_p = 0.131\,V$, $I_p = 0.139\,A$, $R_p = 0.720\,\Omega$, $T_{H,p} = 298.9\,K$, and $T_{L,p} = 294.5\,K$ are calculated numerically, which shows that the optimal value β_p is larger than the manufacturer's structural parameter $2.96\times10^{-3}\,m$. Meanwhile, the maximum efficiency $\eta_{max} = 0.369\%$ and the optimal values $\beta_\eta = 0.309\times10^{-3}\,m$, $V_\eta = 0.242\,V$, $I_\eta = 0.018\,A$, $R_\eta = 8.88\,\Omega$, $T_{H,\eta} = 299.8\,K$, and $T_{L,\eta} = 291.8\,K$ are similarly calculated. The optimal value β_η is very small, which may impacts the thermocouple material's lifetime. Selecting the structural parameter in the range of $\beta_p \le \beta \le \beta_\eta$ can make the system exhibit high performance. Although the obtained maximum efficiency η_{max} is too small, it is still significance for developing the RC-TEG system, because it generates electricity at room temperature and can be applied to power supply for some special equipments and occasions. Based above analysis, the optimal loads at p_{max} and η_{max} can be, respectively, determined as $R_{Load,p} = V_p/I_p = 0.942\,\Omega$ and $R_{Load,\eta} = V_\eta/I_\eta = 13.4\,\Omega$. Adjusting the load resistance in the region of $R_{Load,p} \sim R_{Load,\eta}$, the RC-TEG system can present high performance. Based on the values of $R_{Load,p}$, R_p, $R_{Load,\eta}$, and R_η, the result $R_{Load,\eta}/R_\eta > R_{Load,p}/R_p > 1$ is occurred due to the irreversible thermal losses of the TEG.

4. Conclusions

The RC-TER and RC-TEG systems have been further studied in this work. The main research results are listed as follows:

(1) Under the conditions of daytime and nighttime, the calculated critical temperatures increase with increase of the natural connective coefficient. The critical temperatures at day

time are larger than those in nighttime.

(2) The building's temperature in the RC-TER system is much less than that of the single RC system. For a fixed $A_S/A_T = 100$, the electrical current is optimized to obtain the maximum COP $\psi_m = 4.85$ and the maximum CPD $q_{L,m} = 9.64\times10^3\ \mathrm{W\cdot m^{-2}}$. By Comparing to the single RC system, the SU and the CF electrical current are given. Making trade-off between the COP and CPD, the optimal regions of the current and the hot- and cold-sides' temperatures are determined. The effects of the area ratio A_S/A_T on the RC-TER system are revealed. Increasing A_S/A_T can improve the systems' performance, while the enhancement is not significant as A_S/A_T is increased to the large values.

(3) In the nighttime, the CP2–127–06 Melcor module works as a TEG module. The maximum power density $p_{max} = 5.10\ \mathrm{W\cdot m^{-2}}$ and the maximum efficiency $\eta_{max} = 0.369\%$ and the corresponding optimum conditions are obtained.

The results obtained here may provide basis for thermal managements of the daytime system and power generation in the nighttime.

Acknowledgements

This work has been supported by the Scientific Research Foundation (Grant No. 2019ZD22) and the Teaching Reform and Practice Project (Grant No. 2020YB29) of Chongqing University of Technology, the Science and Technology Research Program of Chongqing Municipal Education Commission (Grant No. KJQN201901144), and the Chongqing Research Program of Basic Research and Frontier Technology (cstc2020jcyjmsxmX0001), People's Republic of China. M. NI also thanks the financial support by Hong Kong Polytechnic University (Project ID: P0014036, account: G-YW3T).

References

[1] Raman A P, Abou Anoma M, Zhu L, Rephaeli E, Fan S. Passive radiative cooling below ambient air temperature under direct sunlight. Nature 2014, 515(7528): 540–544.

[2] Yin X, Yang R, Tan G, Fan S. Terrestrial radiative cooling: Using the cold universe as a renewable and sustainable energy source, Science 2020, 370: 786–791.

[3] Liu T J, Takahara J. Ultrabroadband absorber based on single-sized embedded metal-dielectric-metal structures and application of radiative cooling. Opt. Express 2017, 25(12): A612–A627.

[4] Zhu L, Raman A P, Fan S. Radiative cooling of solar absorbers using a visibly transparent photonic crystal thermal blackbody. Proc. Natl. Acad. Sci. U.S.A. 2015, 112(40): 12282–12287.

[5] Zhao B, Hu M, Ao X, Chen N, Xuan Q, Jiao D, Pei G. Performance analysis of a hybrid system combining photovoltaic and nighttime radiative cooling. Appl. Energy 2019, 252: 113432.

[6] Zhao B, Hu M, Ao X, Pei G. Performance analysis of enhanced radiative cooling of solar cells based on a commercial silicon photovoltaic module. Solar Energy 2018, 176: 248–255.

[7] Zhao D, Yin X, Xu J, Yang R. Radiative sky cooling-assisted thermoelectric cooling system for building applications. Energy 2020, 190: 116322.

[8] Kwan T H, Zhao B, Liu J, Pei G. Performance analysis of the sky radiative and thermoelectric hybrid cooling system. Energy 2020, 10: 117516.

[9] Ishii S, Dao T D, Nagao T. Radiative cooling for continuous thermoelectric power generation in day and night. Appl. Phys. Lett. 2020, 117(1): 013901.

[10] Fan L, Li W, Jin W, Orenstein M, Fan S. Maximal nighttime electrical power generation via optimal radiative cooling. Optics Express 2020, 28(17): 25460–25470.

[11] Zhao B, Pei G, Raman AP. Modeling and optimization of radiative cooling based thermoelectric generators. Appl. Phys. Lett. 2020, 117(16): 163903.

[12] Liu J, Zhang J, Yuan J, Zhang D, Xing J, Zhou Z. Model development and performance evaluation of thermoelectric and radiative cooling module to achieve all-day power generation. Solar Energy Materials & Solar Cells 2021, 220: 110855.

[13] Mu E, Wu Z, Wu Z, Chen X, Liu Y, Fu X, Hu Z. A novel self-powering ultrathin TEG device based on micro/nano emitter for radiative cooling. Nano Energy 2019, 55: 494–500.

[14] Zhan Z, ElKabbash M, Li Z, Li X, Zhang J, Rutledge J, Singh S, Guo C. Enhancing thermoelectric output power via radiative cooling with nanoporous alumina. Nano Energy 2019, 65: 04060.

[15] Jalil S A, ElKabbash M, li Z, Zhang J, Singh S, Zhan Z, Guo C, Multipronged heat-exchanger based on femtosecond laser-nano/microstructured Aluminum for thermoelectric heat scavengers. Nano Energy 2020, 75: 104987.

[16] Jalil S A, Lai B, ElKabbash M, Zhang J, Garcell E M, Singh S, Guo C. Spectral absorption control of femtosecond laser-treated metals and application in solar-thermal devices. Light: Science & Applications 2020, 9(1): 1–9.

[17] https://en.wikipedia.iwiki.uk/wiki/Thermoelectric_cooling#/media/File:Peltierelement.png

[18] Yang, Long L, Meng S, Denisuk N, Chen G, Wang L, Zhu Y. Bulk material based selective infrared emitter for sub-ambient daytime radiative cooling. Solar Energy Materials & Solar Cells 2020, 211: 110548.

[19] Sun X, Sun Y, Zhou Z, Alam M A, Bermel P. Radiative sky cooling: fundamental physics, materials, structures, and applications. Nanophotonics 2017, 6(5): 997–1015.

[20] Riffat S B, Ma X, Wilson R. Performance simulation and experimental testing of a novel thermoelectric heat pump system. Appl. Thermal Eng. 2006, 26: 494–501.

[21] Liao T, He Q, Xu Q, Dai Y, Cheng C, Ni M. Coupling properties and parametric optimization of a photovoltaic panel driven thermoelectric refrigerators system. Energy 2021, 220: 119798.

[22] Liao T, He Q, Xu Q, Dai Y, Cheng C, Ni M. Performance evaluation and optimization of a perovskite solar cell-thermoelectric generator hybrid system. Energy 2020, 201: 117665.

List of Table and Figures

Table 1. Parameters of CP2-127-06 Melcor TER [19].

Hot side temperature T_{H}	300.15 K	308.15 K	323.15 K
$\dot{Q}_{\mathrm{C,max}}\left(\Delta T=0\right)$	117.8	121.4	127.7
$Q_{\mathrm{Cmax}}\left(\Delta T=0\right)$	70.5	73.5	78.8
$I_{\max}\left(\mathrm{A}\right)$	14.2	14.2	14
$V_{\max}\left(\mathrm{V}\right)$	13.9	14.4	15.4
Maximum Operating Temperature	350.15		

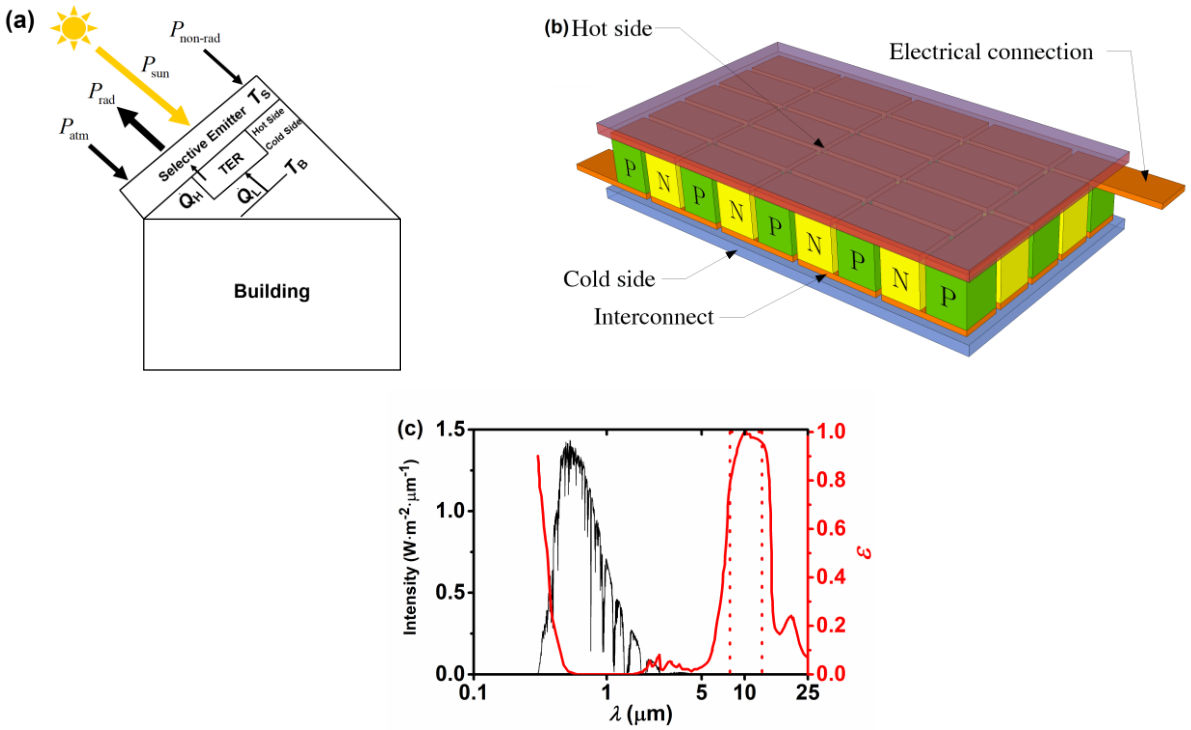

Fig. 1. (a) the schematic diagram of a RC assisted TER system, (b) the structure diagram of a TER [17], and (c) the dependences of thermal emissivity and the AM1.5G solar spectrum on the photon wavelength [18].

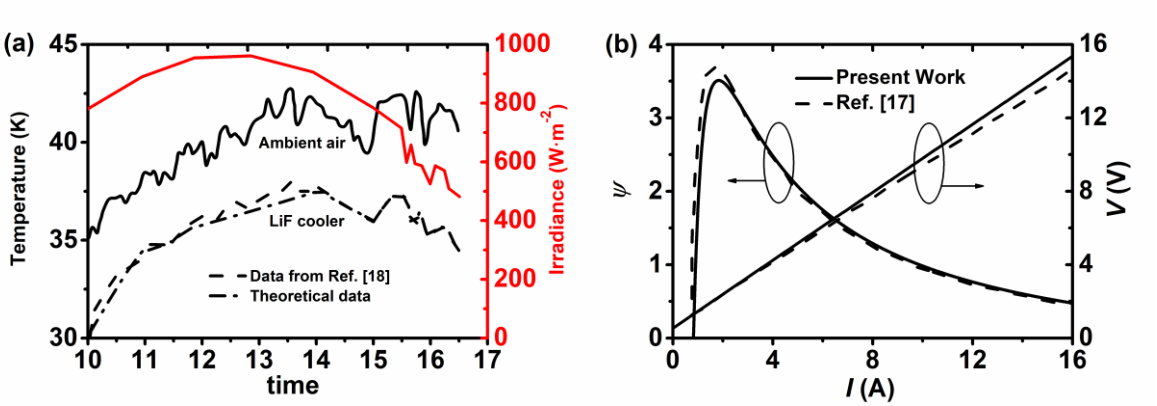

Fig. 2. (a) the solar irradiation and the ambient temperature and the measured and theoretical temperatures of the LiF-based RC cooler and (b) the model validation of the TER's COP and volt-ampere characteristics.

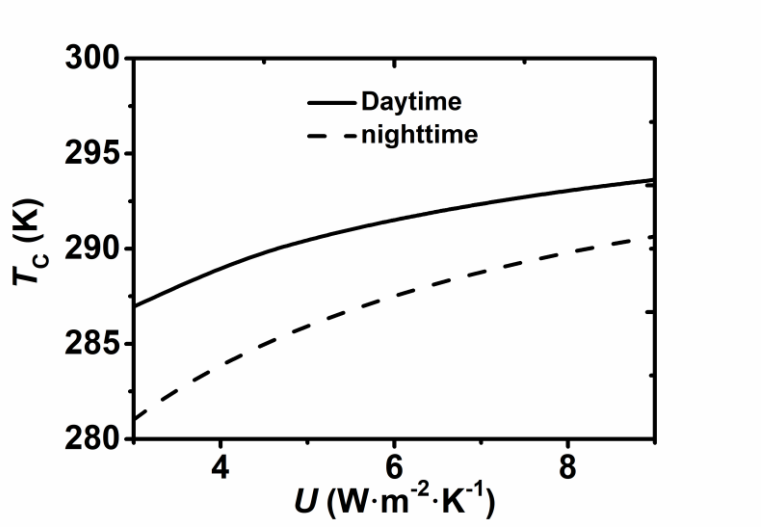

Fig. 3. The curves of selective emitter's temperature as a function of the natural convection coefficient under the conditions of daytime (standard AM1.5G solar spectrum) and nighttime, where the parameters $T_{\mathrm{atm}} = 280\,\mathrm{K}$, $T_{\mathrm{A}} = 300\,\mathrm{K}$ are chosen.

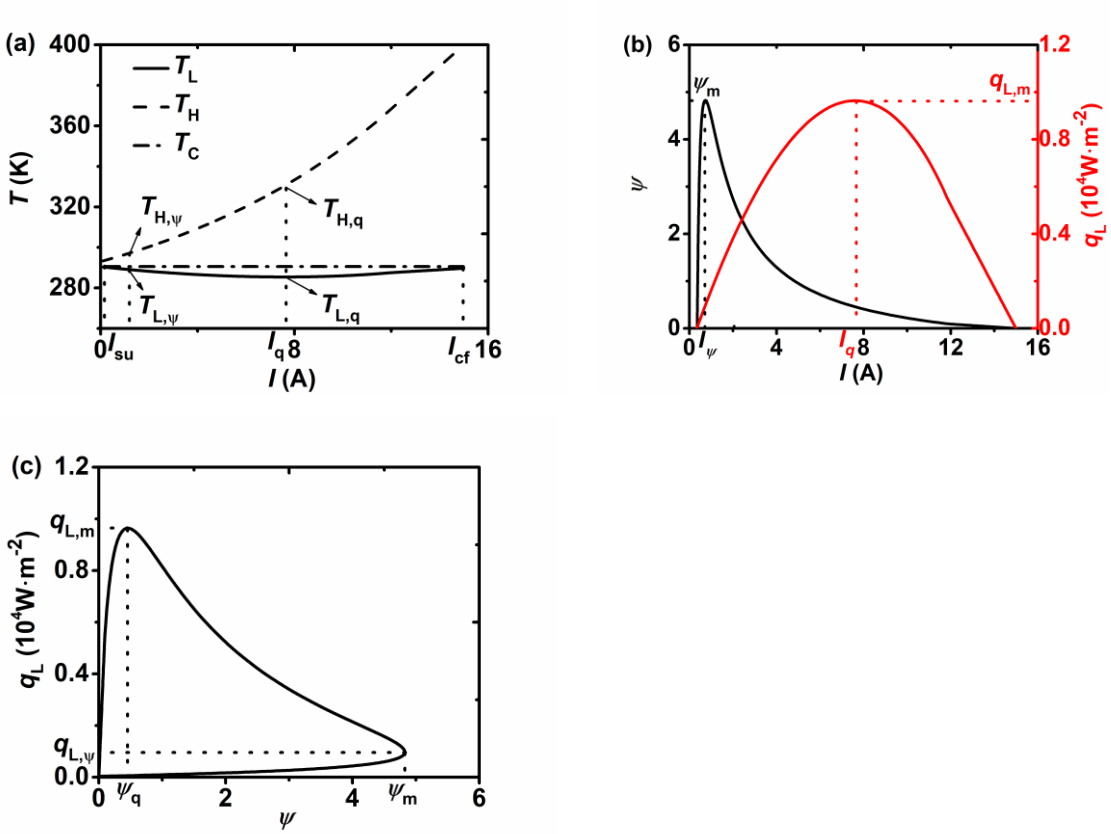

Fig. 4. The curves of (a) the critical temperature T_{C} and the temperatures T_{H} and T_{L} on the hot-side and cold-side of the TER and (b) the COP ψ and the cooling heat flow density CPD q_{L} as a function of the electrical current I, and the q_{L} as a function of ψ, where $U=5\,\mathrm{W\cdot m^{-2}\cdot K^{-1}}$, $T_{\mathrm{B}}=290\,\mathrm{K}$, $A_{\mathrm{S}}/A_{\mathrm{T}}=100$, and $\beta=2.96\times10^{-3}\,\mathrm{m}$.

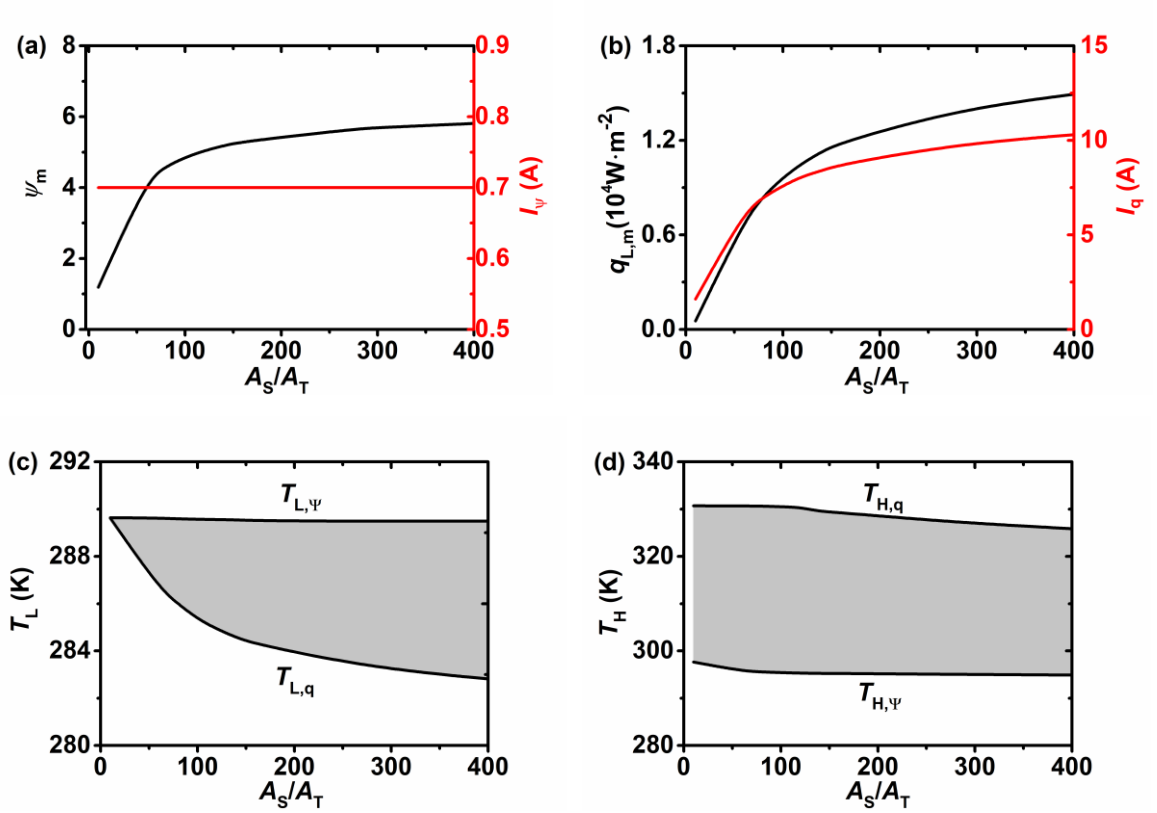

Fig. 5. the curves of (a) the maximum COP $\psi_{\max}$ and the optimal electrical current I_ψ, (b) the maximum CPD $q_{\mathrm{L,m}}$ and the optimal electrical current I_{q}, (c) the temperature $T_{\mathrm{L},\psi}$ at $\psi_{\max}$ and the temperature $T_{\mathrm{L,q}}$ at $q_{\mathrm{L,m}}$, and (d) the temperature $T_{\mathrm{H},\psi}$ at $\psi_{\max}$ and the temperature $T_{\mathrm{H,q}}$ at $q_{\mathrm{L,m}}$ as a function of the area ratio $A_{\mathrm{S}}/A_{\mathrm{T}}$.

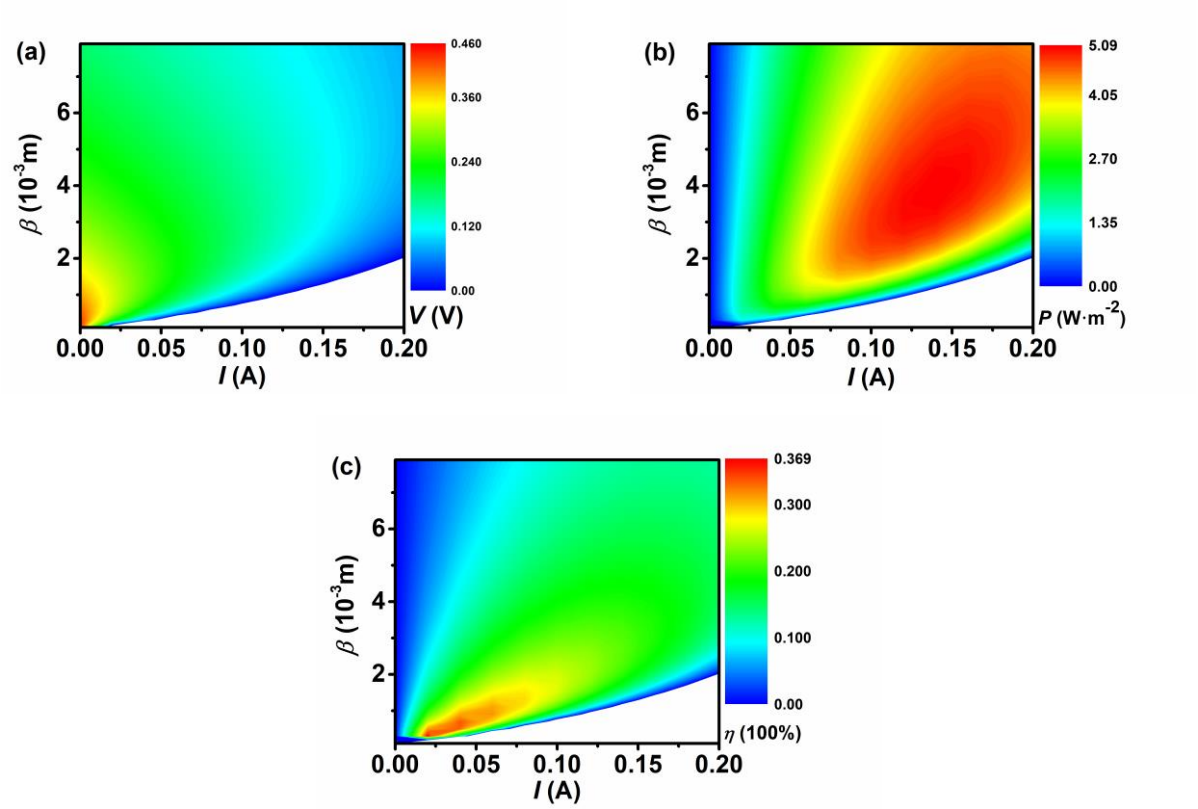

Fig. 6. Three-dimensional projection graphs of (a) the operating voltage V, (b) power density p, and (c) energy conversion efficiency η varying with geometry parameter β and the electrical current I, where $T_A = T_B = 300\,\mathrm{K}$, $A_S / A_\Gamma = 100$.